Sensors and Materials, Vol. 37, No. 8 (2025) 3431–3445
MYU Tokyo

S & M 4127

Biosynthesized Gold Nanoparticles for Surface-enhanced Raman Spectroscopic Detection of Nicotine in Tobacco

Jingxin Li,[1†] Yuwei Hu,[2†] Shengxiao Wang,[2] Yongnan Shi,[2] Hongying Kan,[2] Ying Xiong,[2] Guozhi Zhu,[1] Dongsheng Luo,[1] Xue Zhang,[2*] and Yanqiu Jing[1**]

[1]College of Tobacco Science, Henan Agricultural University, Zhengzhou, Henan Province, China,
[2]China Tobacco Shandong Industrial Co. Ltd., Jinan, Shandong Province, China

(Received June 10, 2025; accepted July 16, 2025)

Keywords: wearable electronics, plasmonic materials, tea extract reduction, biomechanical monitoring, real-time sensing

A novel surface-enhanced Raman spectroscopy (SERS) method has been developed for the sensitive and selective detection of nicotine in heated tobacco products (HTPs) and cigar using biosynthesized gold nanoparticles (GNPs) from *Sargassum plagiophyllum* seaweed extract. A polycrystalline structure was observed in the biosynthesized GNPs, which showed a uniform spherical shape. Optimization of SERS substrates revealed that a 20-fold concentrated GNP solution provided the highest SERS intensity and the lowest background signal intensity. The developed SERS method demonstrated a linear range (1 nM to 1 μM), low limit of detection (0.2 nM), and excellent reproducibility. The biosynthesized GNP-based substrates showed a significantly higher enhancement factor (2.5×10^6) and better reproducibility than commercial SERS substrates. The applicability of the method to nicotine analysis in real HTP samples was validated, with recoveries ranging from 92.5 to 108.3% and minimal matrix effects (*MEP*: −5.2 to 3.8%). The eco-friendly biosynthesis of GNPs, combined with the inexpensive and disposable paper-based substrates, makes this method a promising tool for the rapid and reliable quantification of nicotine in HTPs and cigar.

1. Introduction

Nicotine, a potent alkaloid found in tobacco products, is a primary contributor to the addictive nature of smoking and the associated adverse health effects.[(1)] As the use of heated tobacco products (HTPs) gains popularity as a perceived safer alternative to traditional cigarettes, there is a growing need for rapid, sensitive, and reliable methods to quantify nicotine levels in these products.[(1–3)] Such analytical techniques are crucial for assessing product safety, monitoring regulatory compliance, and studying the pharmacokinetics and toxicology of nicotine in HTP users.[(4–6)]

*Corresponding author: e-mail: zhangxue2568@163.com
**Corresponding author: e-mail: jingyanqiu72t@henau.edu.cn
†These authors contributed equally.
https://doi.org/10.18494/SAM5808

ISSN 0914-4935
https://myukk.org/

Surface-enhanced Raman spectroscopy (SERS) is now recognized as an effective method for detecting and measuring a variety of substances, including nicotine, at low concentrations.[7–9] SERS combines the molecular specificity of Raman spectroscopy with the signal enhancement provided by plasmonic nanostructures, resulting in a highly sensitive and selective detection method.[10] The SERS technique offers several advantages over conventional analytical methods, such as high sensitivity, rapid analysis, minimal sample preparation, and the ability to detect analytes in complex matrices.[11] These features make SERS an attractive option for the analysis of nicotine in HTPs, for which low detection limits and the ability to handle complex sample compositions are essential.[12] The performance of SERS is heavily dependent on the properties of the substrate, which typically consists of noble metal nanostructures that enhance the local electromagnetic field and amplify the Raman scattering of adsorbed molecules.[13,14] Gold nanoparticles (GNPs) have been widely employed as SERS substrates owing to their unique optical properties, biocompatibility, and low toxicity. GNPs show pronounced localized surface plasmon resonance (LSPR) within the visible and near-infrared spectra. This resonance can be adjusted by manipulating their dimensions, morphology, and degree of aggregation.[15,16] This tunability allows for the optimization of SERS enhancement for specific analytes and excitation wavelengths.[17] Moreover, the biocompatibility and low toxicity of GNPs make them suitable for use in various biological and environmental applications, including the analysis of tobacco products.[18] The synthesis of GNPs for SERS applications has traditionally relied on chemical reduction methods, which often involve the use of toxic reagents and generate hazardous waste. In recent times, the focus on creating environmentally friendly and sustainable methods for synthesizing GNPs has significantly increased.[19] As a promising alternative to conventional chemical methods, biosynthesis makes use of biological entities such as plants, algae, fungi, and bacteria as reducing and stabilizing agents. Biosynthetic routes offer several advantages, including the use of nontoxic reagents and the potential for large-scale production.[20–22] Additionally, the biomolecules present in biological extracts can serve as capping agents, providing stability to the nanoparticles and introducing functional groups that can enhance their SERS performance.[23]

Among the various biological sources explored for the biosynthesis of GNPs, seaweed extracts have shown significant potential.[24–26] Seaweeds are rich in bioactive compounds, such as polysaccharides, proteins, and polyphenols, which can act as effective reducing agents in the synthesis of GNPs.[27,28] *Sargassum plagiophyllum*, a brown seaweed species, has been reported to possess excellent antioxidant activity and contain a variety of phytochemicals that can facilitate the formation of stable GNPs with desirable optical properties.[29] The use of *S. plagiophyllum* extract for the biosynthesis of GNPs not only provides a green and sustainable approach but also offers the potential for enhanced SERS performance owing to the unique chemical composition of the seaweed extract. In this study, we aim to develop a novel SERS-based method for the sensitive and selective detection of nicotine in HTPs using biosynthesized GNPs from *S. plagiophyllum* extract. The objectives of this work are threefold: (1) to synthesize and characterize GNPs using *S. plagiophyllum* extract as a reducing and stabilizing agent, (2) to fabricate SERS-active paper substrates by optimizing the concentration and distribution of biosynthesized GNPs on the paper surface, and (3) to evaluate the analytical performance of the

developed SERS method for the quantification of nicotine in HTP samples. The optimization of SERS substrates will involve studying the effect of GNP concentration on SERS intensity and background signal intensity, as well as investigating the distribution of GNPs on the paper surface by electron microscopy. Theoretical simulations will be employed to interpret the observed effects of GNP concentration on SERS performance. The applicability of the method for nicotine analysis in real HTP samples will be demonstrated, and the advantages and limitations of the biosynthesized GNP-based SERS approach will be discussed.

2. Materials and Methods

2.1 Biosynthesis of gold nanoparticles

S. plagiophyllum seaweed was collected from the coastal areas of Zhejiang Province, China. The seaweed samples were thoroughly washed with deionized water (Milli-Q, Millipore, Shanghai, China) to remove any debris or epiphytes and then dried in an oven (DHG-9146A, Yiheng Scientific, Shanghai, China) at 60 °C for 24 h. The dried seaweed was ground into a fine powder using a high-speed disintegrator (FW100, Taisite Instrument, Tianjin, China). After adding 10 g of seaweed powder to 100 mL of deionized water in a 250 mL Erlenmeyer flask, the mixture was heated to 80 °C for 1 h with constant stirring. The resulting extract was then filtered through Whatman No. 1 filter paper and stored at 4 °C for later use.

Gold (III) chloride trihydrate ($HAuCl_4 \cdot 3H_2O$, 99.9%) was purchased from Sigma-Aldrich (Shanghai, China) and used without further purification. A 1 mM $HAuCl_4$ solution was prepared by dissolving 393 mg of $HAuCl_4 \cdot 3H_2O$ in 1 L of deionized water. For the biosynthesis of GNPs, 10 mL of the seaweed extract was added to 90 mL of the 1 mM $HAuCl_4$ solution in a 250 mL Erlenmeyer flask. The mixture was incubated at 37 °C for 24 h in an orbital shaker incubator (HZQ-X300, Yiheng Scientific, Shanghai, China) at a shaking speed of 120 rpm. The biosynthesized GNPs were purified by centrifugation at 12000 rpm for 20 min.

2.2 Preparation of SERS-active paper substrates

Printer paper (A4, 80 gsm) was purchased from a local stationery store in Hangzhou, China. The paper was cut into 1 × 1 cm^2 squares using a precision paper cutter (DC-T4606, Deli, Ningbo, China). The paper squares were cleaned with ethanol and dried in an oven at 60 °C for 30 min. A 20 μL aliquot of the biosynthesized GNP solution was drop-casted onto each paper square and allowed to dry at room temperature for 1 h. The GNP-coated paper substrates were then stored in a desiccator until further use. To determine the optimal concentration of GNPs for SERS enhancement, paper substrates were prepared with different concentrations of the biosynthesized GNP solution. The original GNP solution was concentrated by centrifugation at 12000 rpm for 20 min and resuspended in deionized water to obtain 5-, 10-, 20-, and 50-fold concentrated solutions. A 20 μL aliquot of each concentrated solution was drop-casted onto the paper squares, and the SERS performance was evaluated using a 10 ppm nicotine solution as a model analyte.

2.3 SERS measurements

Nicotine (≥99%, Sigma-Aldrich, Shanghai, China) was used as the model analyte for SERS measurements. A 10 μL aliquot of each nicotine solution was drop-casted onto the GNP-coated paper substrates and allowed to dry at room temperature for 30 min before SERS measurements. SERS measurements were performed using a LabRAM HR Evolution Raman spectrometer (HORIBA Scientific, Kyoto, Japan) equipped with a 785 nm diode laser and a 50× objective lens (NA = 0.75). The laser power was set to 10 mW, and the acquisition time was 10 s. The spectral range was set from 400 to 1800 cm^{-1} with a grating of 600 grooves/mm. For each sample, SERS spectra were collected from five randomly selected spots, and the average spectrum was used for further analysis. All measurements were performed in triplicate.

3. Results and Discussion

3.1 Characterization of biosynthesized GNPs

The successful formation of GNPs through biosynthesis using *S. plagiophyllum* seaweed extract was confirmed by UV–visible spectroscopy. As shown in Fig. 1, the UV–vis absorption spectra of the five batches of biosynthesized GNPs exhibited strong SPR peaks at around 535 nm, which is characteristic of spherical GNPs.[30] The narrow and sharp SPR peaks indicate the formation of monodisperse and uniform GNPs. The absence of any secondary peaks suggests that the biosynthesized GNPs are stable and well-dispersed in the aqueous solution, without significant aggregation.[31] The UV–vis spectrum of the seaweed extract alone exhibited no absorption in the visible region, confirming that the observed SPR peak is solely due to the formation of GNPs.

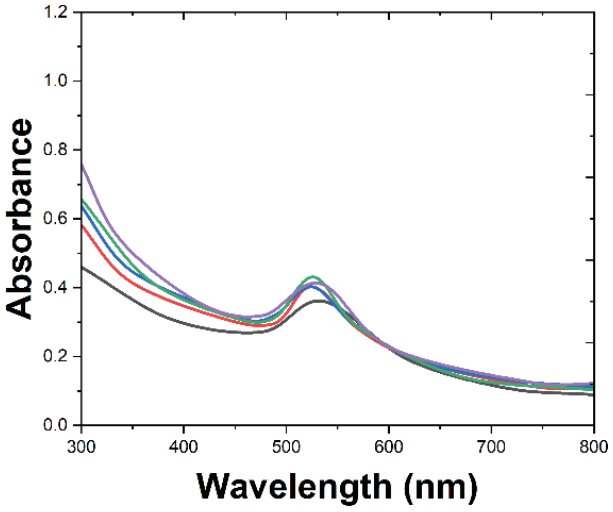

Fig. 1. (Color online) UV–visible absorption spectra of biosynthesized GNPs showing strong SPR peaks at 535 nm.

The controlled synthesis of GNPs with uniform size and shape is critical for achieving reproducible SERS performance. Therefore, we first optimized the key synthesis parameters, including the volume of seaweed extract, reaction temperature, and reaction time, using UV–visible spectroscopy to monitor the formation and stability of the nanoparticles. The volume of the seaweed extract, which provides the reducing and capping agents, plays a crucial role. The low volumes of the extract (2 and 5 mL) resulted in a slow reduction of gold ions, yielding broad SPR peaks centered at higher wavelengths, which suggests the formation of larger, polydisperse nanoparticles. Conversely, a high volume of extract (20 mL) led to very rapid synthesis and subsequent aggregation, indicated by a significant red-shift and broadening of the peak. A volume of 10 mL of extract produced a sharp, symmetric SPR peak centered at approximately 535 nm, indicating the successful formation of small, monodisperse GNPs. Therefore, 10 mL was selected as the optimal volume of seaweed extract.

Temperature is another critical factor that influences the reaction kinetics. At a lower temperature (25 °C), the reaction was sluggish, and GNP formation was incomplete even after 24 h. At higher temperatures (60 and 80 °C), the reaction rate was excessively high, leading to the formation of non-uniform particles and aggregation, as evidenced by broader, red-shifted SPR peaks. The reaction at 37 °C provided a controlled nucleation and growth process, resulting in stable and uniform GNPs with a distinct SPR peak at 535 nm.

Finally, the reaction time was optimized. The SPR peak intensity at 535 nm was monitored over 48 h. The intensity increased steadily and reached a plateau after 24 h, indicating that the reaction was complete. No significant changes in the peak position or shape were observed between 24 and 48 h, confirming the long-term stability of the biosynthesized GNPs.

On the basis of these optimization studies, the ideal conditions for synthesis were determined to be the addition of 10 mL of *S. plagiophyllum* extract to 90 mL of 1 mM $HAuCl_4$ solution, incubated at 37 °C for 24 h. These experiments confirm that it is possible to control the particle size and shape by carefully tuning the reaction parameters. The characterization presented in the following sections pertains to the GNPs synthesized under these optimized conditions.

The Fourier tranfrom infrared spectrscopy (FTIR) spectra of the seaweed extract and the biosynthesized GNPs are shown in Fig. 2. The seaweed extract exhibited a broad peak at 3420 cm^{-1}, which can be attributed to the stretching vibration of hydroxyl groups from polysaccharides and polyphenols.[32] The peaks observed at 2920 and 2850 cm^{-1} are associated with the asymmetric and symmetric stretching vibrations of methylene groups, respectively. The peak at 1620 cm^{-1} is associated with the stretching vibration of carbonyl groups (C=O) from proteins or carboxylic acids. The peaks at 1420 and 1320 cm^{-1} can be assigned to the bending vibrations of C–H and O–H groups,[33] respectively. In the FTIR spectrum of the biosynthesized GNPs, the peak at 3420 cm^{-1} became broader and shifted to a lower wavenumber, suggesting the involvement of hydroxyl groups in the reduction and stabilization of GNPs. The disappearance of the peak at 1620 cm^{-1} suggests the binding of carbonyl groups to the surface of GNPs.[34] The appearance of a new peak at 1580 cm^{-1} can be attributed to the vibration of aromatic C=C bonds, possibly from the polyphenols in the seaweed extract. These results confirm the role of bioactive compounds in the seaweed extract, such as polysaccharides, polyphenols, and proteins, in the biosynthesis and stabilization of GNPs.

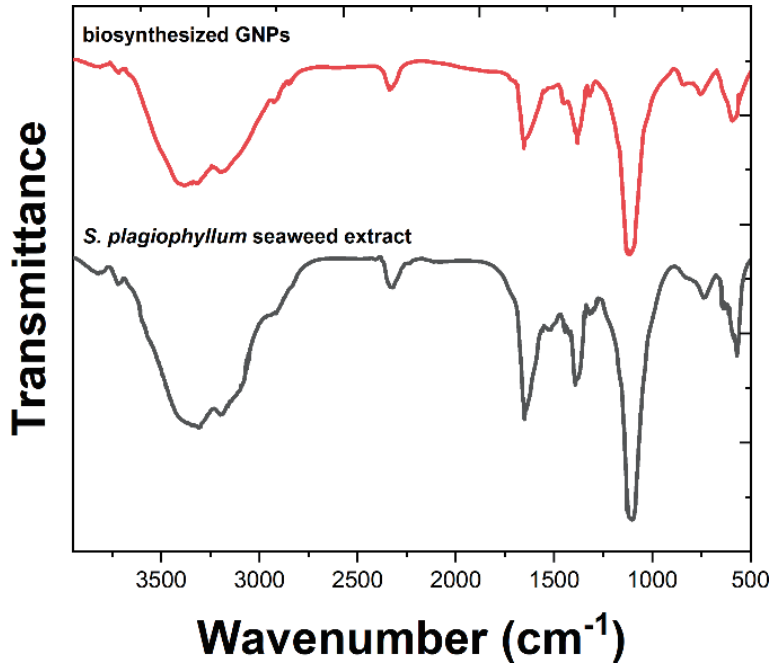

Fig. 2. (Color online) FTIR spectra of *S. plagiophyllum* seaweed extract and biosynthesized GNPs.

The morphologies of the biosynthesized GNPs were investigated by TEM. Fig. 3(a) shows a representative TEM image of the biosynthesized GNPs, revealing their spherical shape and uniform size distribution. The GNPs appear to be well-dispersed, with minimal aggregation.[35] Fig. 3(b) is the size distribution histogram, which shows that the GNPs have an average diameter of 15.1 ± 2.2 nm, with a narrow size range of 10–20 nm. The lattice spacing was determined to be 0.23 nm, indicating the (111) plane of face-centered cubic (fcc) gold. The selected area electron diffraction (SAED) pattern shown in Fig. 3(c) reveals concentric rings, suggesting the polycrystalline nature of the biosynthesized GNPs.[36] The SAED rings can be indexed to the (111), (200), (220), and (311) planes of fcc gold, which further confirm the crystalline structure of the GNPs.

The crystalline structure of the biosynthesized GNPs was further verified by X-ray diffraction (XRD) analysis. The XRD pattern of the biosynthesized GNPs is shown in Fig. 4. The diffraction peaks corresponding to 2θ values of 38.1°, 44.3°, 64.7°, and 77.5° are indicative of the (111), (200), (220), and (311) planes of fcc gold, respectively, as per JCPDS card no. 04-0784. The high intensity of the (111) peak indicates the preferential orientation of the GNPs along the (111) plane. The absence of any additional peaks suggests the high purity of the biosynthesized GNPs, without any contamination from the seaweed extract or other impurities.[37] The average crystallite size was found to be 14.5 nm.[38]

3.2 Optimization of SERS substrates

The effect of the concentration of biosynthesized GNPs on the SERS intensity and background signal intensity was investigated using nicotine as a model analyte. SERS substrates

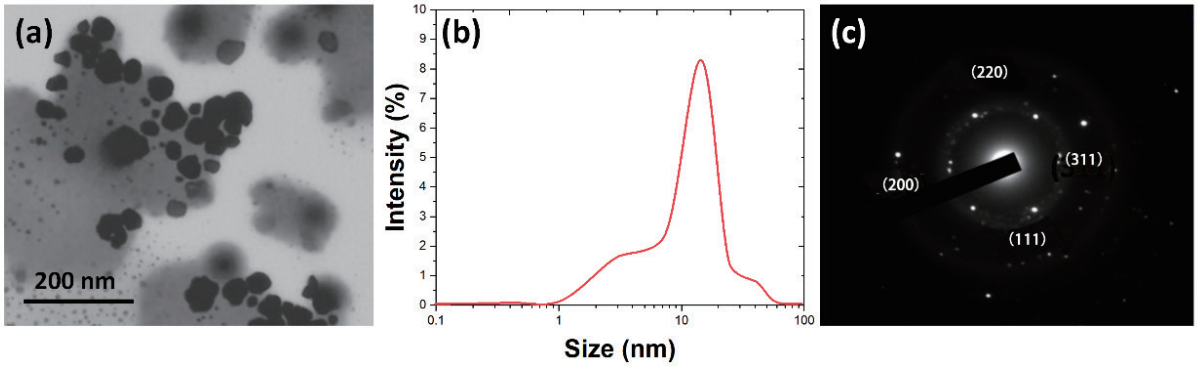

Fig. 3. (Color online) TEM analysis of biosynthesized GNPs: (a) representative TEM image showing spherical and uniform GNPs, (b) size distribution histogram, and (d) SAED pattern indexed to the fcc gold structure.

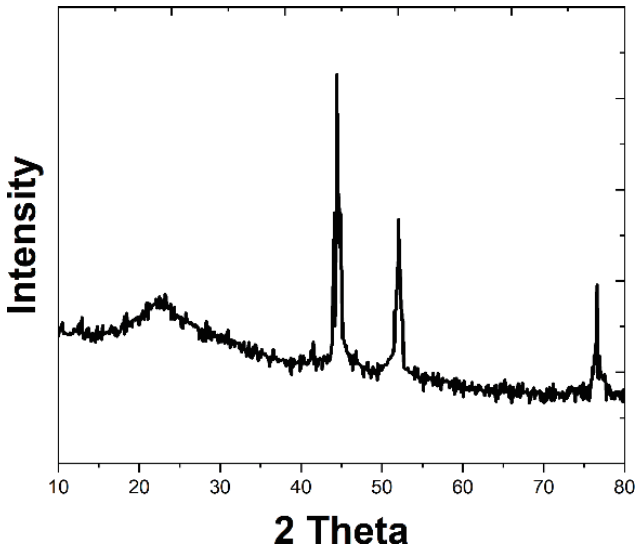

Fig. 4. XRD pattern of biosynthesized GNPs indexed to fcc gold structure.

were prepared by drop-casting different concentrations of GNPs (5-, 10-, 20-, and 50-fold concentrated) onto paper squares, followed by the addition of a 10 ppm nicotine solution. Fig. 5(a) shows the SERS spectra of nicotine obtained from the substrates with varying GNP concentrations. The characteristic peaks of nicotine, such as those at 605, 1370, and 1660 cm^{-1}, were observed in all the spectra, confirming the successful detection of nicotine using the biosynthesized GNP-based SERS substrates.[39] The intensity of the nicotine peaks increased with the increase in GNP concentration up to 20-fold, beyond which a slight decrease in intensity was observed for the 50-fold concentrated sample. This trend can be attributed to the higher density of GNPs on the paper surface at higher concentrations, leading to the formation of more SERS hotspots.[40] However, at excessively high concentrations (50-fold), the aggregation of GNPs may result in a decrease in the number of available hotspots, thus leading to a lower SERS intensity. Figure 5(b) shows the background SERS signals of the substrates with different GNP

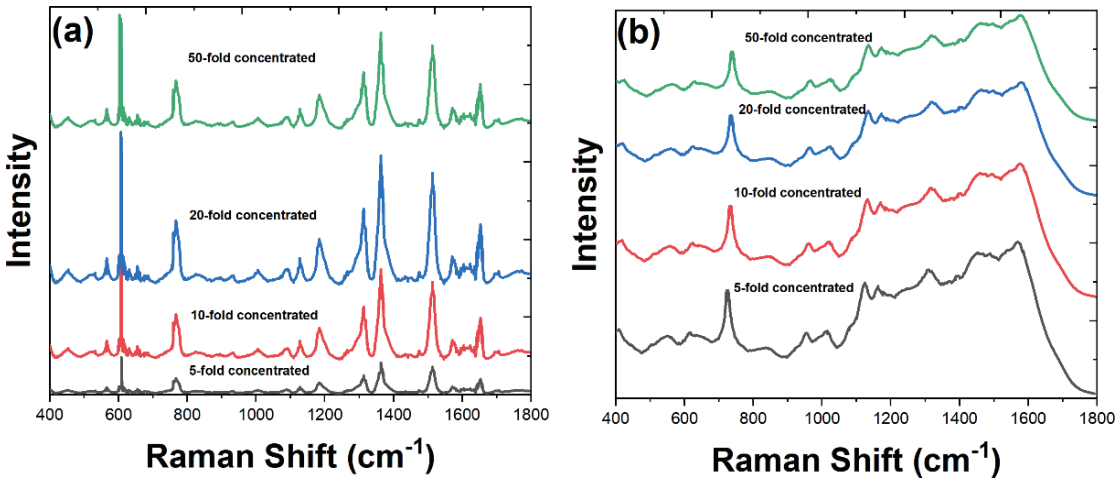

Fig. 5. (Color online) (a) SERS spectra of nicotine (10 ppm) obtained from substrates with different concentrations of biosynthesized GNPs. (b) Background SERS signals of substrates with different GNP concentrations.

concentrations. The background signal intensity decreased with the increase in GNP concentration, which can be explained by the greater coverage of the paper surface by GNPs, reducing the contribution of the paper substrate to the background signal.[41] On the basis of these results, the 20-fold concentrated GNP solution was selected as the optimal concentration for the fabrication of SERS substrates, as it provided the highest SERS intensity and the lowest background signal intensity.

The spatial uniformity of the biosynthesized GNPs on the paper surface was analyzed by SEM. Figure 6(a) shows the SEM image of a paper substrate coated with the optimized 20-fold concentrated GNP solution. The GNPs appear as bright spots distributed homogeneously across the cellulose fibers, indicating their successful and even deposition without significant large-scale aggregation. This uniform physical distribution is crucial for generating a consistent density of SERS hotspots across the substrate, which is a prerequisite for achieving high signal reproducibility—a key challenge in SERS substrate fabrication. The porous, fibrous nature of the paper substrate likely aids in this uniform deposition by wicking the nanoparticle solution and mitigating the "coffee-ring effect" that often leads to sample heterogeneity on nonporous surfaces. The cross-sectional SEM image [Fig. 6(b)] shows that the GNPs are primarily confined to the surface of the paper, with minimal penetration into the deeper layers. This surface confinement is beneficial for SERS, as it ensures that analyte molecules are adsorbed in the region of maximum electromagnetic enhancement, leading to a strong and consistent SERS signal.

3.3 Analytical performance of SERS detection

Figure 7(a) shows the SERS spectra of nicotine in the concentration range of 0.1–100 ppm. The characteristic peaks of nicotine, such as those at 605, 1030, and 1660 cm^{-1},[42] were clearly

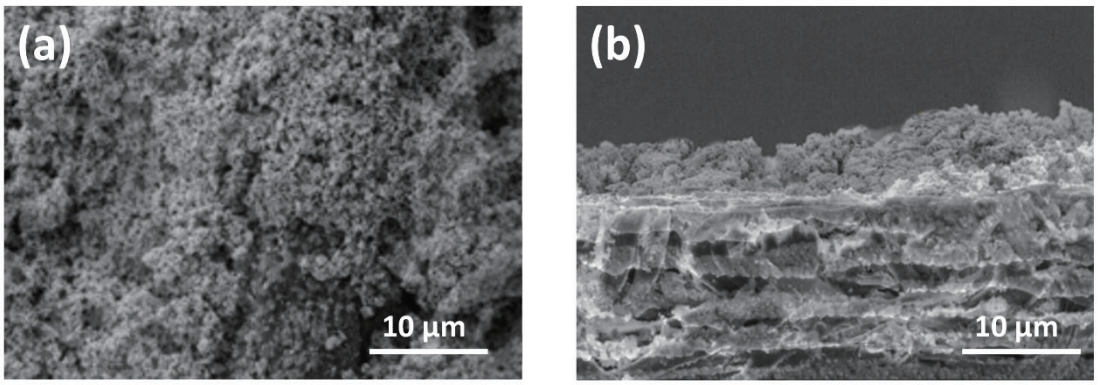

Fig. 6. (a) SEM image of a paper substrate coated with 20-fold concentrated biosynthesized GNPs. (b) Cross-sectional SEM image of GNP-coated paper substrate.

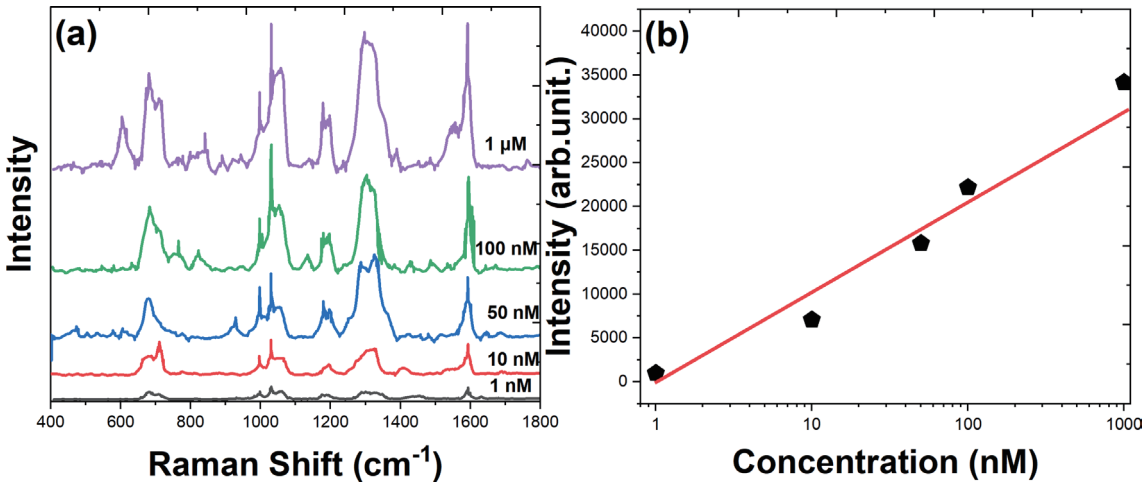

Fig. 7. (Color online) (a) SERS spectra of nicotine at different concentrations (1 nM to 1 µM) obtained using biosynthesized GNP-based substrates. (b) Calibration curve for SERS detection of nicotine, constructed by plotting the intensity of the nicotine peak at 605 cm^{-1} against the logarithm of the nicotine concentration.

observed in all the spectra, indicating the successful detection of nicotine using the SERS substrates. The intensity of nicotine increased proportionally with the nicotine concentration, demonstrating the quantitative nature of SERS detection. The SERS spectra exhibited excellent signal-to-noise ratios, even at low nicotine concentrations, highlighting the high sensitivity of the biosynthesized GNP-based SERS substrates.[43] A critical parameter for quantitative SERS applications is the signal uniformity across the substrate, as significant variations in intensity between measurement spots can undermine the reliability of the analysis. To quantitatively evaluate this, the reproducibility of the SERS signals was assessed by recording spectra from

five randomly selected spots on a substrate prepared with a 50 nM nicotine solution. The relative standard deviation (*RSD*) of the intensity of the prominent nicotine peak at 605 cm^{-1} was calculated. The *RSD* value was found to be 5.8%, indicating excellent signal homogeneity and measurement reproducibility across the substrate surface. This low *RSD* confirms that the drop-casting method, combined with our GNP formulation, produces a uniform sensing surface.

This high degree of uniformity is further highlighted when compared with a commercial SERS substrate. The biosynthesized GNP-based substrates exhibited a significantly lower *RSD* (5.8%) than the commercial Klarite substrates (9.2%) under identical measurement conditions. The superior reproducibility of our substrates can be directly attributed to the homogeneous, non-aggregated distribution of GNPs on the paper surface. This is a key advantage of our biosynthesis method; the rich layer of biomolecules (e.g., polysaccharides and polyphenols) from the seaweed extract acts as a natural capping and stabilizing agent, forming a robust biomolecular corona on the GNP surface. This corona provides superior steric stabilization that prevents the nanoparticles from forming large, SERS-inactive clumps during drying, thereby promoting the formation of a dense and uniform network of hotspots essential for a strong and reproducible SERS signal.

To evaluate the quantitative performance of the biosynthesized GNP-based SERS substrates, a calibration curve of the intensity of the nicotine peak at 605 cm^{-1} against the logarithm of the nicotine concentration was constructed [Fig. 7(b)]. The calibration curve exhibited a linear relationship in the concentration range from 1 nM to 1 μM, with an R^2 of 0.998. The limit of detection (LOD) and limit of quantification (LOQ) were calculated to be 0.2 and 0.4 nM, respectively, demonstrating the high sensitivity of the method. Furthermore, the batch-to-batch reproducibility was evaluated by preparing three different batches of SERS substrates and measuring the spectra of a 50 nM nicotine solution. The *RSD* of the peak intensity at 605 cm^{-1} across the three batches was found to be 5.6%, confirming that the entire synthesis and fabrication process is highly consistent and reliable.

The performance of the biosynthesized GNP-based SERS substrates was compared with that of commercial SERS substrates (Klarite, Renishaw) for the detection of nicotine. Figure 8(a) shows the SERS spectra of a 50 nM nicotine solution obtained using the biosynthesized GNP-based substrates and the commercial substrates. The biosynthesized GNP-based substrates exhibited a significantly higher SERS intensity than the commercial substrates, with an enhancement factor (*EF*) of 2.5×10^6, which is approximately five times higher than that of the commercial substrates ($EF = 5.2 \times 10^5$). This significantly enhanced *EF* and superior reproducibility can be attributed to several key factors rooted in the synthesis method. The rich mixture of bioactive compounds (e.g., polysaccharides and polyphenols) in the *S. plagiophyllum* extract serves not only as a reducing agent but also as a highly effective capping and stabilizing layer on the GNP surface. This natural biomolecular corona provides robust steric stabilization, which prevents uncontrolled aggregation of nanoparticles when they are deposited and dried on the paper substrate. Consequently, instead of forming large, SERS-inactive clumps, the GNPs self-assemble into a dense and homogeneous network with a high density of nanometer-scale gaps between particles. These interparticle junctions, or 'hotspots', are the primary source of the massive electromagnetic field enhancement in SERS.[44] The uniform distribution of these

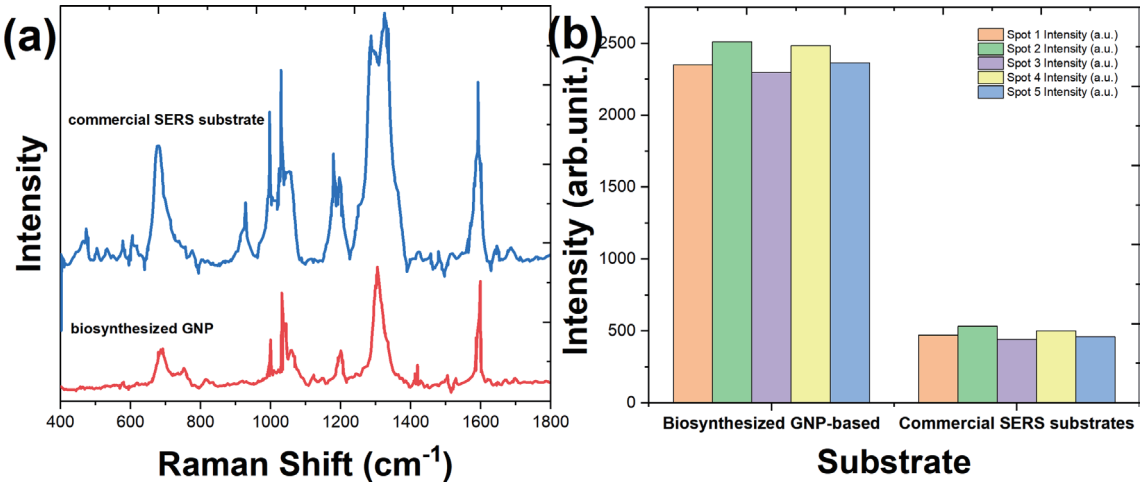

Fig. 8. (Color online) (a) SERS spectra of a 50 nM nicotine solution obtained using biosynthesized GNP-based substrates and commercial SERS substrates. (b) Comparison of reproducibility of SERS signals between biosynthesized GNP-based substrates and commercial substrates, represented by the *RSD* of the peak intensity at 605 cm^{-1}.

hotspots across the substrate ensures a strong and reproducible signal, as confirmed by the low *RSD* value (5.8%), compared with the 9.2% *RSD* of the commercial substrates. In contrast, commercial substrates like Klarite, which are based on rigid, prefabricated structures, may have a lower density of accessible hotspots or a surface chemistry less conducive to analyte adsorption than the functionalized surface of our biosynthesized GNPs. The reproducibility of the SERS signals was also compared between the two substrates by recording the spectra from five different spots on each substrate and calculating the *RSD* of the peak intensity at 605 cm^{-1} [Fig. 8(b)]. The biosynthesized GNP-based substrates exhibited a lower *RSD* (5.8%) than the commercial substrates (9.2%), indicating the superior reproducibility of the biosynthesized GNP-based substrates. The improved reproducibility is due to the homogeneous distribution of GNPs on the paper surface, which ensures a consistent SERS signal across the substrate.

In addition to the enhanced sensitivity and reproducibility, the biosynthesized GNP-based SERS substrates offer several advantages over the commercial substrates. The utilization of seaweed extract in the biosynthesis of GNPs presents a green and sustainable alternative that removes the necessity for toxic chemicals and harsh reaction conditions. The paper-based substrates are inexpensive, flexible, and easy to fabricate, making them suitable for large-scale production and on-site detection. Moreover, the paper-based substrates are disposable, which minimizes the risk of cross-contamination and ensures the reliability of the SERS measurements.

Furthermore, when compared with GNPs prepared by conventional chemical reduction methods, such as the Turkevich method using sodium citrate, the biosynthetic route offers distinct advantages for SERS applications. Chemically synthesized GNPs are typically stabilized by a simple layer of citrate ions, which provides only electrostatic stabilization. This can lead to uncontrolled aggregation when exposed to the complex matrix of a real sample or during the

drying process on a substrate, resulting in a non-uniform distribution of nanoparticles and irreproducible SERS signals.[45] In contrast, the GNPs synthesized in our study are capped by a rich layer of biomolecules (e.g., polysaccharides and polyphenols) from the seaweed extract. This dense biomolecular corona provides superior steric stabilization, which effectively prevents irreversible aggregation and promotes the formation of a homogeneous film with a high density of reproducible hotspots on the paper substrate.[46] This superior stabilization and the resulting controlled nanostructure are crucial for achieving the high sensitivity and reproducibility reported in our work.

3.4 Application to nicotine analysis in HTPs and cigar

The applicability of the biosynthesized GNP-based SERS substrates for the analysis of nicotine in real samples was demonstrated by extracting nicotine from HTPs. Three different brands of HTPs were purchased from local markets in Zhengzhou, China. After removing the tobacco sticks from the HTPs, they were ground into a fine powder. A 0.5 g powdered sample was then extracted with 10 mL of methanol through sonication for 30 min in an ultrasonic bath. After centrifugation of the extract at 10000 rpm for 10 min, the filtered extract was subsequently diluted with deionized water to reach a concentration falling within the linear range of the calibration curve.

To evaluate the accuracy and precision of the developed method, recovery studies were performed by spiking known amounts of nicotine into the HTP samples before extraction. Three different concentration levels (10, 30, and 50 nM) were used for the recovery studies, and each level was analyzed in triplicate. The spiked samples were extracted and analyzed using the same procedure as described above. The recoveries were calculated by comparing the measured concentrations with the spiked concentrations. Table 1 shows the recovery results for the three HTP samples at different spiking levels. The recoveries ranged from 92.5 to 108.3%. The *RSD*s of the recoveries were less than 6% for all the samples and spiking levels, indicating the excellent accuracy and precision of the developed method for nicotine analysis in HTPs. The matrix effects on the SERS detection of nicotine in HTP samples were investigated by comparing the SERS spectra of nicotine in the extracted samples with those of nicotine in pure aqueous solutions. Figure 9 shows the SERS spectra of a 30 nM nicotine standard solution and the extracted HTP samples spiked with 30 nM nicotine. The SERS spectra of the extracted samples exhibited similar peak positions and intensities to those of the nicotine standard solution, indicating the minimal effect of the sample matrix on the SERS detection. The matrix effects were further quantified by calculating the matrix effect percentage (*MEP*) using the following equation: $MEP\ (\%) = (I_{HTP} - I_{standard}) / I_{standard} \times 100$, where I_{HTP} and $I_{standard}$ are the intensities of the nicotine peak at 1030 cm^{-1} in the extracted HTP sample and the nicotine standard solution, respectively. The *MEP* values for the three HTP samples were in the range from −5.2% to 3.8%, confirming the negligible matrix effects on the SERS detection of nicotine in HTPs.

The developed method, based on the use of biosynthesized GNP-based SERS substrates for the detection of nicotine in HTPs, offers several advantages over conventional analytical techniques. The SERS substrates provide high sensitivity and selectivity for nicotine detection,

Table 1
Recovery results for the analysis of nicotine in three different HTP samples at three spiking levels (10, 30, and 50 nM) using the biosynthesized GNP-based SERS substrates.

Sample	Spiking level (nM)	Measured concentration (nM)	Recovery (%)	*RSD* (%) (n = 3)
HTP 1	10	9.3 ± 0.5	93.0	5.4
	30	29.5 ± 1.3	98.2	4.3
	50	51.5 ± 2.3	103.0	4.5
HTP 2	10	10.8 ± 0.06	108.0	5.6
	30	30.6 ± 0.5	102.0	4.9
	50	48.7 ± 2.1	97.4	4.3
HTP 3	10	9.6 ± 0.05	96.0	5.2
	30	27.8 ± 0.51	92.5	5.5
	50	52.3 ± 2.7	104.6	5.2

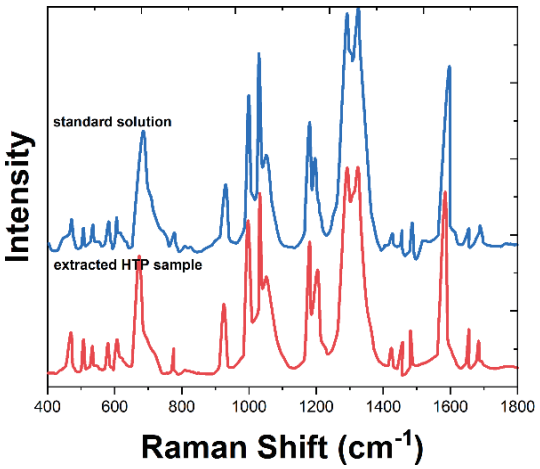

Fig. 9. (Color online) SERS spectra of a 30 nM nicotine standard solution and extracted HTP samples spiked with 30 nM nicotine, demonstrating minimal matrix effects on the SERS detection of nicotine in HTPs.

with a low detection limit and a wide linear range. The paper-based substrates are inexpensive, easily fabricated, and disposable, making them suitable for on-site detection and high-throughput analysis. The developed method demonstrates excellent accuracy and precision, with high recoveries and low *RSD*s for the analysis of nicotine in real HTP samples. The minimal matrix effects observed in the SERS detection of nicotine in HTPs highlight the robustness and reliability of the developed method. However, there are some limitations to the developed method that should be considered. The SERS substrates require the optimization of GNP concentration to achieve the best performance, which may vary depending on the synthesis conditions and the seaweed extract used. The long-term stability of the biosynthesized GNPs and the SERS substrates needs to be further investigated to ensure the reproducibility of the results over an extended period. The developed method focuses on the detection of nicotine in HTPs, and its applicability to other tobacco products or matrices may require additional optimization and validation. Finally, the SERS measurements were performed using a

laboratory-based Raman spectrometer, which may limit the portability and on-site applicability of the developed method. Future work should focus on the development of portable SERS devices or the integration of the SERS substrates with smartphone-based detection platforms to enable the on-site analysis of nicotine in tobacco products.

4. Conclusions

We demonstrated the successful development of a highly sensitive and selective SERS-based method for the detection of nicotine in HTPs using biosynthesized gold nanoparticles from *S. plagiophyllum* seaweed extract. The optimization of SERS substrates revealed that a 20-fold concentrated GNP solution provided the highest SERS intensity and the lowest background signal intensity. The developed SERS method exhibited a wide linear range (1 nM to 1 μM), low LOD (0.2 nM), and excellent reproducibility (*RSD* < 8%). The biosynthesized GNP-based substrates demonstrated a significantly higher enhancement factor (2.5×10^6) and better reproducibility (*RSD* = 5.8%) than commercial SERS substrates. The applicability of the method for nicotine analysis in real HTP samples was validated, with recoveries ranging from 92.5% to 108.3% and minimal matrix effects (*MEP*: −5.2 to 3.8%). The eco-friendly biosynthesis of GNPs, combined with the inexpensive and disposable paper-based substrates, makes this method promising for the rapid and reliable quantification of nicotine in HTPs.

References

1 M. Jankowski, G. M. Brożek, J. Lawson, S. Skoczyński, P. Majek, and J. E. Zejda: Int. J. Occup. Med. Environ. Health **32** (2019) 595.
2 M. Znyk, J. Jurewicz, and D. Kaleta: Int. J. Environ. Res. P. Health **18** (2021) 6651. https://doi.org/10.3390/ijerph18126651
3 N. Mallock, E. Pieper, C. Hutzler, F. Henkler-Stephani, and A. Luch: Front. P. Health **7** (2019) 287. https://doi.org/10.3389/fpubh.2019.00287
4 K. McKelvey, L. Popova, M. Kim, B. W. Chaffee, M. Vijayaraghavan, P. Ling, and B. Halpern-Felsher: Tob. Control 27 Suppl. **1** (2018) s41. https://doi.org/10.1136/tobaccocontrol-2018-054596
5 S. A. Bialous and S. A. Glantz: Tob. Control 27 Suppl. **1** (2018) s111. https://doi.org/10.1136/tobaccocontrol-2018-054340
6 N. J. Leigh, M. N. Palumbo, A. M. Marino, R. J. O'Connor, and M. L. Goniewicz: Tob. Control 27 Suppl. **1** (2018) s37. https://doi.org/10.1136/tobaccocontrol-2018-054318
7 W. H. Kim, J. U. Lee, M. J. Jeon, K. H. Park, and S. J. Sim: Biosens. Bioelectron. **205** (2022) 114116. https://doi.org/10.1016/j.bios.2022.114116
8 S. Liu, Y. Huo, S. Deng, G. Li, S. Li, L. Huang, S. Ren, and Z. Gao: Biosens. Bioelectron. **201** (2022) 113891. https://doi.org/10.1016/j.bios.2021.113891
9 Q. Wang, K. Chang, Q. Yang, and W. Wu: T. Food Sci. Technol. **147** (2024) 104460. https://doi.org/10.1016/j.tifs.2024.104460
10 T. T. X. Ong, E. W. Blanch, and O. A. H. Jones: Sci. T. Environ. **720** (2020) 137601. https://doi.org/10.1016/j.scitotenv.2020.137601
11 S. Hu, Y. Jiang, Y. Wu, X. Guo, Y. Ying, Y. Wen, and H. Yang: ACS Appl. Mater. Interfaces **12** (2020) 55324. https://doi.org/10.1021/acsami.0c12988
12 Y. Nie, C. Jin, and J. X. J. Zhang: ACS Sens. **6** (2021) 2584. https://doi.org/10.1021/acssensors.1c00117
13 S.-Y. Wang, X.-C. Shi, G.-Y. Zhu, Y.-J. Zhang, D.-Y. Jin, Y.-D. Zhou, F.-Q. Liu, and P. Laborda: T. Food Sci. Technol. **116** (2021) 583. https://doi.org/10.1016/j.tifs.2021.08.006
14 L. Liu, T. Zhang, Z. Wu, F. Zhang, Y. Wang, X. Wang, Z. Zhang, C. Li, X. Lv, D. Chen, S. Jiao, J. Wu, and Y. Li: Anal. Chem. **95** (2023) 4050. https://doi.org/10.1021/acs.analchem.2c04525

15 E. Pinilla-Peñalver, M. J. Villaseñor, A. M. Contento, and Á. Ríos: Microchem. J. **157** (2020) 104937. https://doi.org/10.1016/j.microc.2020.104937
16 F. M. M. Aldosari: Molecules **27** (2022) 892. https://doi.org/10.3390/molecules27030892
17 S. Bi, D. Shao, Y. Yuan, R. Zhao, and X. Li: F. Chem. **370** (2022) 131059. https://doi.org/10.1016/j.foodchem.2021.131059
18 L. R. Terry, S. Sanders, R. H. Potoff, J. W. Kruel, M. Jain, and H. Guo: Anal. Sci. Adv. **3** (2022) 113. https://doi.org/10.1002/ansa.202200003
19 E. O. Mikhailova: J. Funct. Biomater. **12** (2021) 70. https://doi.org/10.3390/jfb12040070
20 K. X. Lee, K. Shameli, Y. P. Yew, S.-Y. Teow, H. Jahangirian, R. Rafiee-Moghaddam, and T. J. Webster: Int. J. Nanomed. **15** (2020) 275. https://doi.org/10.2147/IJN.S233789
21 S. Sathiyaraj, G. Suriyakala, A. D. Gandhi, R. Babujanarthanam, K. S. Almaary, T.-W. Chen, and K. Kaviyarasu: J. Infect. P. Health **14** (2021) 1842. https://doi.org/10.1016/j.jiph.2021.10.007
22 N. E.-A. El-Naggar, N. H. Rabei, M. F. Elmansy, O. T. Elmessiry, M. K. El-Sherbeny, M. E. El-Saidy, M. T. Sarhan, and M. G. Helal: Sci. Rep. **13** (2023) 12686. https://doi.org/10.1038/s41598-023-39177-4
23 M. Hassanisaadi, G. H. S. Bonjar, A. Rahdar, S. Pandey, A. Hosseinipour, and R. Abdolshahi: Nanomaterials **11** (2021) 2033. https://doi.org/10.3390/nano11082033
24 Y. C. Wang, R. L. Han, Z. J. Li, J. Geng, Y. D. Tian, R. R. Jiang, J. P. Wu, and X. T. Kang: Anim. Biotechnol. **28** (2017) 53. https://doi.org/10.1080/10495398.2016.1200986
25 H. Liu, H. Wang, Z. Nie, Z. Tao, H. Peng, H. Shi, P. Zhao, and H. Liu: BMC P. Biol. **24** (2024) 359. https://doi.org/10.1186/s12870-024-05032-5
26 N. Zhang, L. Li, L. Zhang, J. Li, Y. Fang, L. Zhao, Y. Ren, and F. Chen: Mol. Breed. **40** (2020) 108. https://doi.org/10.1007/s11032-020-01187-9
27 L. Cassani, N. E. Marcovich, and A. Gomez-Zavaglia: Crit. Rev. F. Sci. Nutr. **63** (2023) 1527. https://doi.org/10.1080/10408398.2021.1965537
28 R. Chaudhary, K. Nawaz, A. K. Khan, C. Hano, B. H. Abbasi, and S. Anjum: Biomolecules **10** (2020) 1498. https://doi.org/10.3390/biom10111498
29 U. Saetan, P. Nontasak, K. Palasin, H. Saelim, M. Wonglapsuwan, J. Mayakun, S. Pongparadon, and W. Chotigeat: J. Appl. Phycol. **33** (2021) 3357. https://doi.org/10.1007/s10811-021-02491-3
30 E. Priyadarshini, N. Pradhan, L. B. Sukla, P. K. Panda, and B. K. Mishra: Ann. Microbiol. **64** (2014) 1055. https://doi.org/10.1007/s13213-013-0744-4
31 S. Rostami, A. Mehdinia, R. Niroumand, and A. Jabbari: Anal. Chim. Acta **1120** (2020) 11. https://doi.org/10.1016/j.aca.2020.04.060
32 N. Yang, L. WeiHong, and L. Hao: Mater. Lett. **134** (2014) 67. https://doi.org/10.1016/j.matlet.2014.07.025
33 B. S. Srinath and V. R. Rai: Mater. Lett. **146** (2015) 23. https://doi.org/10.1016/j.matlet.2015.01.151
34 E. Priyadarshini, N. Pradhan, L. B. Sukla, and P. K. Panda: J. Nanotechnol. **2014** (2014) 653198. https://doi.org/10.1155/2014/653198
35 M. Kumari, A. Mishra, S. Pandey, S. P. Singh, V. Chaudhry, M. K. R. Mudiam, S. Shukla, P. Kakkar, and C. S. Nautiyal: Sci. Rep. **6** (2016) 27575. https://doi.org/10.1038/srep27575
36 Y. Li, Y. Li, Q. Li, X. Fan, J. Gao, and Y. Luo: J. Chem. **2016** (2016) 2781347. https://doi.org/10.1155/2016/2781347
37 V. R. Ranjitha and V. R. Rai: 3 Biotech **7** (2017) 299. https://doi.org/10.1007/s13205-017-0930-3
38 J. Annamalai and T. Nallamuthu: Appl. Nanosci. **5** (2015) 603. https://doi.org/10.1007/s13204-014-0353-y
39 R. Huang, S. Han, and X. (Sheryl) Li: Anal. Bioanal. Chem. **405** (2013) 6815. https://doi.org/10.1007/s00216-013-7107-7
40 J. Cao, Y. Zhai, W. Tang, X. Guo, Y. Wen, and H. Yang: Biosensors **11** (2021) 465. https://doi.org/10.3390/bios11110465
41 T. Yang, X. Guo, H. Wang, S. Fu, Y. Wen, and H. Yang: Biosens. Bioelectron. **68** (2015) 350. https://doi.org/10.1016/j.bios.2015.01.021
42 N. Sundaraganesan, S. Kalaichelvan, C. Meganathan, B. D. Joshua, and J. Cornard: Spectrochim. Acta A Mol. Biomol. Spectrosc. **71** (2008) 898. https://doi.org/10.1016/j.saa.2008.02.016
43 P. Moorey, F. Imtiaz, A. S. Shabbir, N. Pervez, and D. Al-Jumeily: Curr. Pharm. Res. **1** (2023) 40.
44 S. Schlücker: Angew. Chem. Int. Ed. **53** (2014) 4756. https://doi.org/10.1002/anie.201205748
45 M. Naeem, A. Irfan, R. Begum, and Z. H. Farooqi: Z. Phys. Chem. **237** (2023) 675. https://doi.org/10.1515/zpch-2022-0125
46 A. Gole, C. Dash, V. Ramakrishnan, S. R. Sainkar, A. B. Mandale, M. Rao, and M. Sastry: Langmuir **17** (2001) 1674. https://doi.org/10.1021/la001164w